Scientific Reports

https://doi.org/10.1038/s41598-026-35007-5

Article in Press

High-frequency characteristics analysis and optimization of coaxial-like TGVs

Received: 11 October 2025

Accepted: 1 January 2026

Published online: 07 January 2026

Cite this article as: Chen S., Wang J., Liu X. *et al.* High-frequency characteristics analysis and optimization of coaxial-like TGVs. *Sci Rep* (2026). https://doi.org/10.1038/s41598-026-35007-5

Shouwei Chen, Jin Wang, Xingpeng Liu, Xiaoping Wu, Jie Liu & Dawen Xia

High-Frequency Characteristics Analysis and Optimization of Coaxial-Like TGVs

Shouwei Chen [1,2,*,#], Jin Wang[3,4,#], Xingpeng Liu [3,4], Xiaoping Wu[1,2], Jie Liu[5], Dawen Xia[1,2]

[1] School of Microelectronics and Artificial Intelligence, Kaili University, Kaili 556011, China;

[2] Micro-nano and Intelligent Manufacturing Engineering Research Centre of Ministry of Education, Kaili 556011, China;

[3] Guilin University Of Electronic Technology, Guilin 541004, China;

[4] Guangxi Key Laboratory of Precision Navigation Technology and Application, Guilin University of Electronic Technology, Guilin 541004, China;

[5] Qiandongnan Polytechnic College, Kaili 556011, China;

* Corresponding author: Shouwei Chen, achengshouwei@163.com

[#]These authors contributed equally to this work.

Abstract: The Coaxial-Like through-glass vias (TGVs) are frequently used vertical interconnect transmission structures in radio frequency (RF) three-dimensional(3D) integrated circuits (ICs). This paper addresses the TGV's structure in high-density 3D packaging by proposing a multi-parameter co-optimization methodology that integrates electromagnetic modeling, response surface methodology (RSM), and genetic algorithm (GA), significantly enhancing its high-frequency transmission performance. Innovatively, a 3D full-wave electromagnetic simulation model of the coaxial-like TGV is established to systematically analyze the influence of via pitch *p*, via radius *r*, and number of ground vias n on the insertion loss S21. An analytical model for RLGC parasitic parameters based on electromagnetic theory is derived. A second-order response surface model correlating S21 with key structural parameters is constructed via Box-Behnken experimental design, and globally optimized using a genetic algorithm, resulting in an optimized parameter set (p = 82.05 μm, r = 10.44 μm, n = 10) for S21 at 100 GHz. Simulation results verify that the optimized S21 improves by 0.0052 dB compared to the baseline model, with a relative enhancement of 21.94%. This study not only provides a theoretical foundation and optimization framework for high-performance TGV design, but also offers an effective solution for low-loss interconnects in 3D integrated RF devices.

Keywords: Coaxial-Like through-glass vias; high-frequency characteristics; insertion loss; structural optimization.

1. Introduction

As chip fabrication technology continues to approach the physical limits of Moore's Law, three-dimensional (3D) packaging technology has become one of the key pathways for sustaining chip performance improvement, thanks to its significant advantages in enhancing integration density, reducing power consumption, and achieving heterogeneous integration [1]. Emerging application scenarios such as 5G communication, artificial intelligence, high-performance computing, and advanced optoelectronic systems have imposed stringent requirements on packaging and interconnect technologies that exceed traditional planar integration, necessitating the fulfillment of core criteria such as high-frequency and high-speed signal transmission, ultra-low interconnection latency, and high-reliability packaging. In this context, through-glass-via (TGV) technology is accelerating the shift from laboratory research to industrial application based on its excellent intrinsic material properties and scalable process potential, and is widely regarded as a key enabling technology driving the development of next-generation high-density 3D packaging [2,3].

Although Through-Silicon-Via (TSV) technology has been widely applied in existing 2.5D/3D packaging[4-11], its inherent characteristics of silicon substrate pose severe challenges in high-frequency (especially millimeter-wave band) and high-power application scenarios. The relatively high dielectric constant ($\varepsilon r \approx 11.7$) and loss tangent ($\tan\delta \approx 0.01$) of silicon materials lead to significant signal transmission loss as frequency increases. Simultaneously, the significant mismatch in Coefficient of Thermal Expansion (CTE) between silicon and typical packaging materials can easily induce interfacial stress accumulation and potential failure during thermal cycling, severely restricting the long-term reliability of systems in extreme environments [1,12,13]. This mismatch generates shear stresses at material interfaces during temperature

fluctuations, which can lead to delamination, cracking, or via failure over repeated cycles. In contrast, TGV technology based on low-loss materials such as borosilicate glass and quartz glass exhibits revolutionary advantages: its dielectric constant can be as low as 3.0-4.0, and the loss tangent ($\tan\delta \approx 10^{-4}$ - 10^{-3}) is 1-2 orders of magnitude lower than that of silicon-based materials [14-18], effectively suppressing the skin effect and dielectric loss of high-frequency signals. By precisely controlling the glass composition, good CTE matching with silicon chips (CTE≈3 ppm/K) can be achieved, thereby significantly alleviating thermomechanical stress issues [19-23]. This close CTE match minimizes the differential expansion between the silicon die and the glass interposer during thermal cycling. As a result, interfacial shear and tensile stresses are substantially reduced, which inhibits fatigue-driven failure mechanisms such as crack initiation and propagation, interfacial delamination, and via extrusion. Consequently, systems employing CTE-matched glass interposers demonstrate enhanced long-term reliability under repeated thermal loading, making them suitable for applications subject to wide temperature ranges or power cycling.

However, the basic single-signal through-glass via (TGV) structure still faces significant signal integrity (SI) challenges when transmitting high-frequency signals [24,25], especially in the millimeter-wave and terahertz bands. These challenges mainly include impedance mismatch, electromagnetic field leakage, and increased crosstalk between adjacent channels. To address these bottlenecks, coaxial-like through-glass vias (coaxial-like TGV) offer a promising 3-D integration solution [26], capable of providing reliable and high-performance signal transmission through glass substrates. Structurally, the coaxial-like TGV consists of a central signal via surrounded by multiple ground vias arranged in a circular or polygonal pattern. This configuration fundamentally mitigates the three key challenges faced by standard single signal TGVs: (1) Impedance mismatch: The controlled arrangement of signal and ground vias enables precise tuning of the characteristic impedance (typically targeting 50 Ω) by adjusting geometric parameters such as the pitch-to-radius ratio, which is difficult to achieve with an isolated signal via due to the lack of a well-defined return path. (2) Electromagnetic field leakage: The encircling ground vias act as a distributed electromagnetic shield, confining the electric and magnetic fields within the structure and reducing radiation loss and unintended coupling to adjacent circuits. (3) Inter-via crosstalk: The grounded vias provide electrostatic shielding between neighboring signal paths, significantly attenuating capacitive and inductive coupling, thereby enhancing channel isolation, especially in dense via arrays. LeClair T et al. studied a coaxial-like TGV structure, which demonstrated over 40 dB of crosstalk isolation and a 0.5 dB improvement in insertion loss at 30 GHz compared to standard glass-filled through vias[27]. Boora V et al. conducted a preliminary electrical characteristic and performance analysis of Coaxial-Like TGV using electromagnetic field simulation tools[28]. Kiran K M et al. proposed an equivalent transmission line model for Coaxial-Like TGV, establishing formulas for frequency and temperature-dependent resistance, inductance, capacitance, and admittance based on Bessel and Neumann functions derived from electromagnetic theory[29].

This paper establishes a corresponding simulation model for the Coaxial-Like TGV, proposes a set of universal analytical formulas for the resistance-inductance-capacitance-conductance (RLGC) parasitic parameters, and the corresponding high-frequency equivalent circuit model. This formula system is derived based on the fundamental theory of electromagnetic fields, and the corresponding parasitic parameters can be calculated according to the process dimensions and material properties, providing a theoretical basis for the prediction of electrical performance. On this basis, the model is verified within the 100 GHz frequency band through three-dimensional full-wave simulation. The influence of structural size changes on insertion loss is further explored in combination with the established formulas, and the simulation results show good consistency with the theoretical analysis. Finally, a multi-parameter collaborative optimization strategy combining the response surface method and genetic algorithm is introduced to achieve rapid optimization design of the Coaxial-Like TGV structure with the goal of improving high-frequency transmission performance, providing theoretical support and design reference for the development of high-performance glass transition boards and three-dimensional integrated RF devices.

2. Equivalent Circuit Model

2.1.Coaxial-Like TGV structure and equivalent circuit model

The structure of the Coaxial-Like TGV is shown in Fig. 1, and the dimensional parameters and their symbols are shown in Fig. 2, where the radius of the TGV conductor is *r*, the height of the TGV is *h*, the height of the

substrate is h_{tgv}, the distance between the signal TGV and the grounded TGV is *P*, and the number of grounded TGVs is *n*.

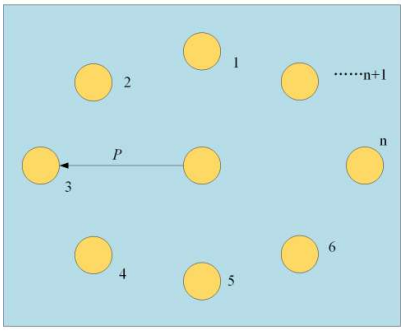

Fig. 1. Coaxial-Like TGV structure.

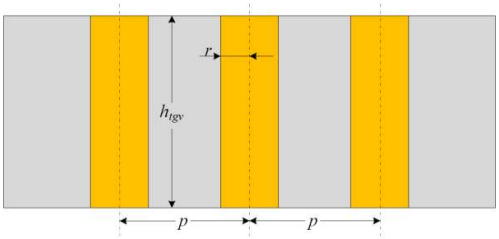

Fig. 2. Dimensional parameters of the Coaxial-Like TGV.

The analysis of TGV's high-frequency characteristics is essentially the solution of a complex electromagnetic field boundary value problem, which can be solved using HFSS software based on the full-wave electromagnetic analysis method of electromagnetic field theory. Fig. 3 shows the TGV simulation model based on HFSS software. This model includes multiple ground vias, a signal via located at the center of the circle, and the upper and lower circular surfaces of the via as excitation ports. The medium in the dielectric layer between the vias is glass, and the outside of the dielectric layer is an ideal boundary condition with air as the medium. This model is a single vertical via structure. The distance from the center of the signal via to the center of the ground via is the via distance, represented by the letter p. The radius of the upper and lower circular surfaces of the via is the via radius, represented by the letter r. The number of ground vias located around the signal via is the number of vias, represented by the letter n. The basic dimensional parameters are: via distance *p* is 120 μm, via radius *r* is 10 μm.

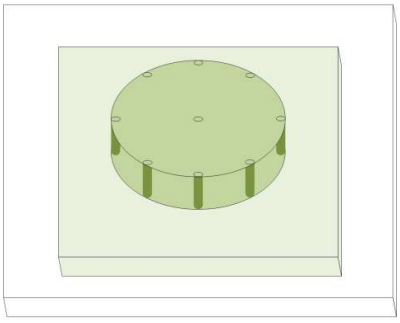

Fig. 3. Coaxial-Like TGV simulation model.

2.2. Extraction of parasitic parameters

2.2.1. Equivalent resistance of current circuit

The equivalent resistance R_g of the current loop is the total resistance of n TGVs connected in parallel and then one TGV connected in series, that is

$$R_g = (1 + \frac{1}{n}) \cdot R_{tgv} \quad (1)$$

In the formula, R_{tgv} represents the resistance of a single TGV. R_{tgv} is composed of a DC component resistance R_{dc} and an AC component resistance R_{ac}, that is

$$R_{tgv} = \sqrt{{R_{dc}}^2 + {R_{ac}}^2} \tag{2}$$

Where R_{dc} can be known from Ohm's law

$$R_{dc} = \frac{h_{tgv}}{\pi \sigma_{tgv} r^2} \tag{3}$$

In the formula, σ_{tgv} represents the conductivity of the TGV conductor material. At high frequencies, current tends to concentrate on the surface of the conductor due to the eddy current effect, known as the skin effect. The skin effect leads to the generation of R_{ac}, that is

$$R_{ac} = \frac{h_{tgv}}{\pi(2r\delta - \delta^2)} \tag{4}$$

In the formula, 'δ' represents the skin depth, that is

$$\delta = \frac{1}{\sqrt{\mu_0 \pi f \sigma_{tgv}}} \tag{5}$$

In the formula: μ_0 represents the vacuum permeability; f denotes the current frequency.

From equations (1) to (5), we can ultimately obtain the equivalent resistance R_g as

$$R_g = \frac{n+1}{n} \cdot \frac{h_{tgv}}{\pi \sigma_{tgv}} \cdot \sqrt{\frac{1}{r^4} + \frac{1}{\delta^2 (2r - \delta)^2}} \tag{6}$$

2.2.2. Equivalent inductance of current loop

In this model, as the operating frequency increases, the influence of parasitic inductance gradually increases, even surpassing that of parasitic resistance. Simultaneously, the skin effect causes current to concentrate more on the outer surface of the conductor. When the operating frequency is very high, there is almost no current inside the conductor, so the internal self-inductance can be neglected. Assuming that the signal TGV is 0#TGV, taking 1#TGV in the figure as the reference current loop, and each grounded TGV as a current loop, a wide separation approximation is applied to the TGV conductor. Assuming that the current flowing out of the signal TGV flows out of the grounded TGV on average, then when the current flowing through 0#TGV is I, the current flowing in from each grounded TGV is I/n. According to the basic theory of electromagnetic fields, the self-inductance of 0#TGV is

$$L_0 = \frac{\mu_0 h_{tgv}}{2\pi} \cdot \ln\ p_r \tag{7}$$

In the formula, pr is an intermediate variable, and p_r=p/r.The self-inductance of 1#TGV is L_1=L_0/n, and the mutual inductance of i-grounded TGV is

$$L_i = \frac{\mu_0 h_{tgv}}{2\pi n} \cdot \ln \frac{p}{p_i} \tag{8}$$

In the formula, pi represents the spacing between i#TGV and 1#TGV, where 2≤i≤n. After simplifying the operation of $\sum_{j=0}^{n} L_j$, we can obtain L_g as follows:

$$L_g = \frac{n+1}{n} \cdot \frac{\mu_0 h_{tgv}}{2\pi} \cdot \ln(k_n p_r) \tag{9}$$

In the formula, k_n represents the structural coefficient, and it is a parameter solely related to the number n of grounded TGVs

$$k_n = \left[\sum_{m=1}^{n-1} \frac{1}{2\sin(m\pi/n)}\right]^{\frac{1}{n+1}} \tag{10}$$

In addition, the relative permeability of all materials mentioned in this article is assumed to be 1 and has been omitted in the formulas.

2.2.3. Equivalent capacitance and equivalent conductance

The equivalent s capacitance C_{sub} of the substrate is

$$C_{sub} = \frac{\mu_0 \varepsilon_{sub} h_{tgv}^2}{L_g} \tag{11}$$

In the formula, ε_{sub} represents the dielectric constant of the substrate material.

By substituting equation (12) into equation (11), we can obtain the equivalent capacitance C_{sub} of the substrate

$$C_{sub} = \frac{n}{n+1} \cdot \frac{2\pi\varepsilon_{sub} h_{tgv}}{\ln(k_n p_r)} \tag{12}$$

The equivalent conductance G_{sub} of the substrate can be calculated using the relationship between capacitance and conductance $C_{sub}/G_{sub}=\varepsilon_{sub}/\sigma_{sub}$, where σ_{sub} represents the conductivity of the substrate material. Thus, we can obtain

$$G_{sub} = \frac{n}{n+1} \cdot \frac{2\pi\sigma_{sub} h_{tgv}}{\ln(k_n p_r)} \tag{13}$$

3. Simulation of high-frequency characteristics of Coaxial-Like TGV

Based on current research on quasi-coaxial structures, the study of high-frequency characteristics of dielectric-layer quasi-coaxial structures on silicon substrates is relatively mature. This paper further constructs a theoretical model of Coaxial-Like TGV on glass substrates based on the theoretical foundation of quasi-coaxial TSV. Using the three-dimensional electromagnetic simulation tool HFSS, the S-parameters of TGV at 1 GHz-100 GHz are extracted, and the S-parameters (S11 and S21) under different structural parameters of Coaxial-Like TGV are obtained. The magnitude of the S-parameters is used as an indicator to evaluate the high-frequency characteristics of Coaxial-Like TGV. The S-parameters describe the reflection performance of signals in the transmission path. A smaller S11 value indicates the better reflection and transmission performance, while a larger S21 value indicates the better high-frequency performance and energy loss. Fig. 4 is a schematic diagram of the planar structure of Coaxial-Like TGV. The glass substrate is made of photosensitive glass material with a dielectric constant of 6.58 and a loss tangent (tan δ) of 0.0086. The radius of the Coaxial-Like TGV is 5 μm, the height is 50 μm, and the spacing between the central TGV and the grounded TGV is 100 μm.

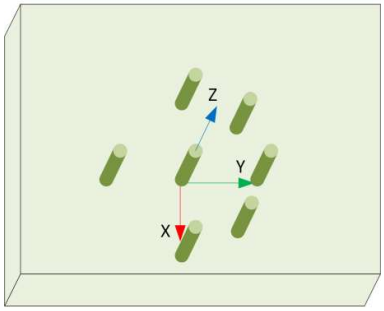

Fig. 4. The Coaxial-Like TGV plane structure diagram.

3.1. Analysis of the influence of through-hole spacing p on Coaxial-Like TGV S21 parameters

Fig. 5 illustrates the impact of varying the distance p between the signal TGV and the grounded TGV on insertion loss. As can be seen from the figure, within the frequency range of 0~100 GHz, insertion loss increases as the spacing p increases. According to equations (12) and (13), an increase in *p* leads to a decrease

in C_{sub}. From equations (7) and (8), it can be observed that an increase in p results in an increase in L_0 and L_i, thereby increasing L_g. This increase in inductance leads to greater loss of the signal during transmission. At low frequencies, L_g and C_{sub} have a minor effect on transmission characteristics. However, as the frequency increases further, the influence of L_g gradually increases, gradually becoming the main factor affecting transmission characteristics. Fig. 6 verifies the aforementioned theory: increasing *p* leads to greater signal loss and a decline in transmission performance. Additionally, the spacing between vias also affects impedance matching. If there is an impedance mismatch, it can cause signal reflection, leading to an increase in the reflection coefficient and subsequently affecting transmission performance.

The dominance of L_g at high frequencies can be understood from the frequency dependence of the equivalent circuit components. The impedance magnitude of the inductive component is given by $Z_L = 2\pi f L_g$, which scales linearly with frequency (f). In contrast, the equivalent resistance R_g is dominated by the AC component R_{ac} at high frequencies due to the skin effect. As shown in equations (4) and (6), $R_{ac} \propto 1/\delta$ and $\delta \propto 1/\sqrt{f}$, leading to $R_g \propto \sqrt{f}$ (from Eq.5). Therefore, as frequency increases, the inductive impedance Z_L grows at a rate proportional to f, while the resistive impedance grows only at a rate proportional to $\sqrt{f}$. This fundamental scaling difference causes the impact of L_g on the overall impedance and signal attenuation to become disproportionately larger at higher frequencies.

Consequently, the increase in L_g with larger p leads to greater signal loss during transmission, especially pronounced in the millimeter-wave band. At low frequencies, R_g and C_{sub} have a more comparable influence on transmission characteristics. However, as the frequency increases beyond approximately 40 GHz, the influence of L_g gradually increases and becomes the dominant factor determining the slope of the S21 curve, as evidenced by the steeper decline in S21 for larger p values in Fig. 5.

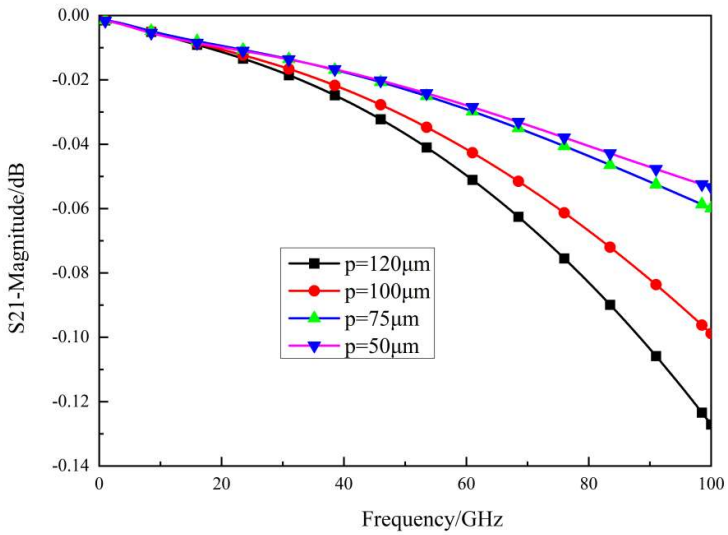

Fig. 5. S21 variation with frequency under different via spacing.

3.2. Analysis of the influence of the through-hole radius r on the Coaxial-Like TGV S21 parameter

Fig. 6 illustrates the impact of changes in the Coaxial-Like TGV conductor radius r on insertion loss when the number of ground vias n, p, and h remain constant. From the figure, it can be observed that as the radius *r* increases, the insertion loss decreases, and the reflection reduces, which is conducive to improving signal integrity. According to Equation (6), due to the presence of the skin effect, an increase in r leads to a decrease in the equivalent resistance of the current loop. The reduction in equivalent resistance is beneficial for reducing insertion loss. From Equations (9) and (13), it can be seen that an increase in r decreases L_g and increases C_{sub}. The increase in equivalent capacitance of the current loop becomes the main factor affecting signal transmission, reducing the hindrance to signal transmission at high frequencies and enhancing the integrity of signal transmission, thereby reducing insertion loss. It is evident that appropriately increasing the diameter of the Coaxial-Like TGV is beneficial for signal transmission. Especially under high-frequency conditions, conductor loss is dominated by the skin effect. Increasing the diameter d can increase the

cross-sectional area, leading to a reduction in conductor loss. Therefore, when increasing the via radius, the high-frequency characteristics of the Coaxial-Like TGV exhibit improved transmission performance. To ensure the transmission performance of high-frequency signals within the Coaxial-Like TGV, the TGV via radius can be appropriately increased when designing the adapter board for chip glass, in order to enhance the high-frequency transmission performance of the Coaxial-Like TGV.

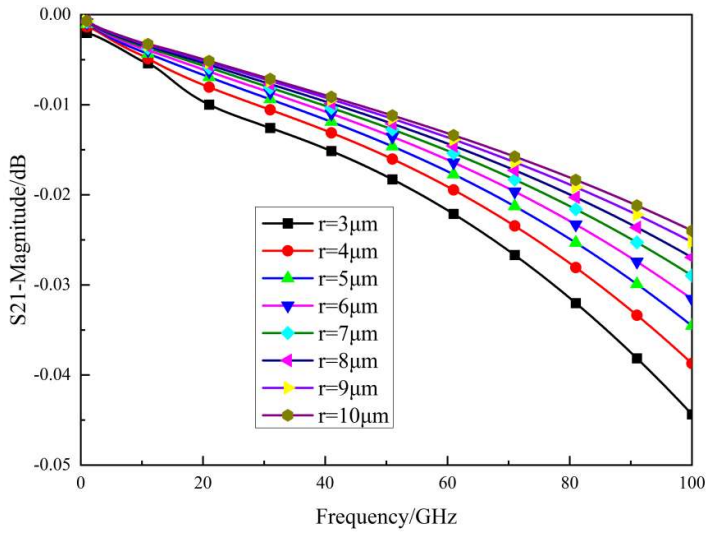

Fig. 6. S21 varies with frequency under different via hole radius

3.3. Analysis of the impact of the number of ground vias, n, on Coaxial-Like TGV S21.

As can be seen from Fig. 7, as the number of peripheral TGV increases, the amplitude of S21 decreases. The number of peripheral TGVs is mainly related to the structural coefficient *kn* in formula (10). When the number *n* is small, such as when n is less than 4, *kn* decreases as *n* increases. However, when *n* exceeds 4, *kn* gradually increases as n becomes larger, gradually approaching 1. For a quasi-coaxial model, the high-frequency band is mainly affected by inductance. According to formula (10), the larger the number *n*, the closer *kn* is to 1, which reduces the inductance of the entire structure and decreases loss. An appropriate increase in the number n enhances the electromagnetic shielding effect of the peripheral grounded TGVs to some extent, thereby improving the transmission effect.

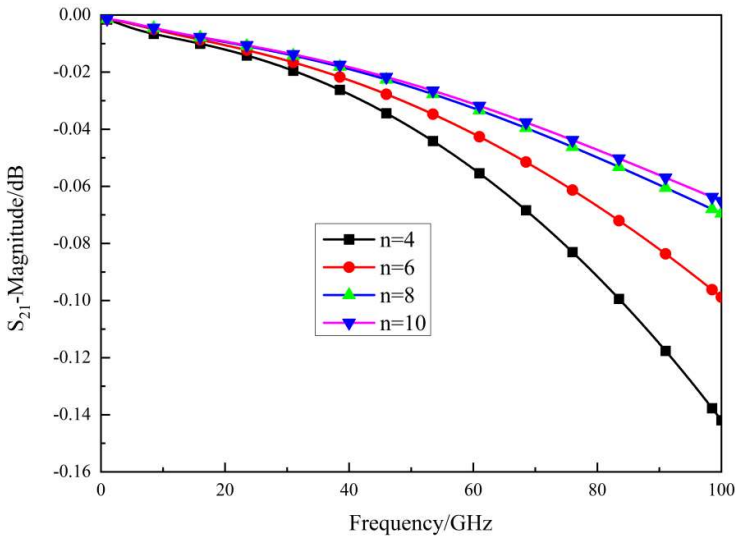

Fig. 7. Variation of S21 with frequency under different numbers of ground vias.

4. Optimization of Coaxial-Like TGV S21

To achieve the most favorable results for Coaxial-Like TGV high-frequency signal transmission, it is necessary to conduct an optimization analysis of the Coaxial-Like TGV structural parameters. By combining the response surface methodology with genetic algorithms, the maximum value of TGV S21 at a signal

frequency of 100 GHz is taken as the optimization objective to obtain the optimal combination of structural parameters for TGV high-frequency signal transmission.

4.1. Response surface methodology

The response surface methodology is a multivariate optimization method based on statistics, designed to efficiently explore the design space of complex systems by establishing a mathematical relationship model between input parameters and output responses. Its core involves constructing a second-order polynomial equation with limited simulation or experimental samples through scientifically designed experiments (Box-Behnken design), quantitatively describing the nonlinear interactions between variables and the patterns of their impact on target performance. This method combines analysis of variance (ANOVA) to verify the significance of the model and utilizes response surface plots or contour plots to visually present the synergistic effects between parameters, thereby quickly locating the optimal solution. Compared to traditional trial-and-error methods, response surface methodology is both efficient and global, widely applied in fields such as antenna design, process parameter optimization, and electromagnetic compatibility analysis, providing data-driven decision support for multi-objective, high-dimensional engineering problems. To ensure methodological transparency and reproducibility, the RSM implementation followed a standardized procedure: (1) Experimental Design: A three-factor, three-level Box-Behnken Design (BBD) was employed for its efficiency in building a second-order model with a minimal number of simulations. (2) Design Points: The design comprised 12 factorial points and 5 center points (replicated runs at the mid-level of all factors, as listed in Table 2), with the latter used to estimate pure experimental error[30,31]. (3) Model Fitting & Validation: The response data (S21 at 100 GHz) from the BBD simulations were fitted to the second-order polynomial model (Eq.14) using least-squares regression. The significance, goodness-of-fit, and predictive ability of the model were rigorously assessed via Analysis of Variance (ANOVA), as detailed in Table 3. Therefore, this paper adopts response surface methodology to establish a functional relationship between the Coaxial-Like TGV S21 and its key structural parameters.

4.2. Simulation experiment design

This article employs the Box-Behnken experimental design method of response surface analysis, which can reduce the number of experiments while meeting experimental requirements. For the key structural parameters of Coaxial-Like TGV, the key factors affecting Coaxial-Like TGV S21 are selected: via spacing *p*, via radius r, and number of ground vias n. Each influencing factor is selected with a maximum and minimum value, and the range of factor values is shown in Table 1. The response surface experimental design includes a total of 17 sets of simulation models, as shown in Table 2. Among them, 12 sets are used as analysis factors, and 5 sets are zero-point factors for experimental error estimation. Corresponding simulation models are established for analysis, and 17 sets of Coaxial-Like TGV S21 values are obtained.

Table 1. Factor Value Table.

Name	Units	Low	High
A(Through-hole spacing p)	μm	50	120
B(The radius of the through hole r)	μm	4	10
C(Number of through holes n)		6	10

Table 2. 17 sets of simulation results from response surface experiments.

Serial number	Via spacing p/μm	Thru-hole radius r/μm	The number of through-holes N	S21/dB
experiment 1	50	4	8	-0.0378
experiment 2	120	4	8	-0.1181
experiment 3	50	10	8	-0.0636
experiment 4	120	10	8	-0.0253
experiment 5	50	7	6	-0.0237
experiment 6	120	7	6	-0.0338
experiment 7	50	7	10	-0.0254

experiment 8	120	7	10	-0.0478
experiment 9	85	4	6	-0.0345
experiment 10	85	10	6	-0.0222
experiment 11	85	4	10	-0.0750
experiment 12	85	10	10	-0.0175
experiment 13	85	7	8	-0.0287
experiment 14	85	7	8	-0.0287
experiment 15	85	7	8	-0.0287
experiment 16	85	7	8	-0.0287
experiment 17	85	7	8	-0.0287

4.3. Response surface analysis

Based on the principles of calculus, any complex function can be approximated and expressed through polynomial segmentation. Therefore, in engineering problems, even if there is a nonlinear relationship between the variables and the target response, polynomial regression can be used for modeling. This article focuses on the nonlinear characteristics of three design variables (via spacing *p*, via radius r, and via count *n*) and the target value (return loss S21). Combining the experimental sample data in Table 1, a second-order polynomial model of Taylor's expansion is selected for fitting. The mathematical expression is as follows:

$$Y = a_0 + \sum_{i=1}^{n} a_i x_i + \sum_{i=1}^{n} a_{ii} x_i^2 + \sum_{i=1}^{n-1} \sum_{j=i+1}^{n} a_{ij} x_i x_j + \in \tag{14}$$

In the equation, a0 represents the baseline response value as a constant term; $\sum a_i x_i$ represents the direct effect of a single variable as a linear term; $\sum a_{ii} x_i^2$ describes the nonlinear effect of variables as a quadratic term; $\sum a_{ij} x_i x_j$ characterizes the interaction between variables as a cross term; and $\in$ denotes the random error term. Through fitting experimental data, a quantitative relationship model between S21 and *p*, *r*, *n* was ultimately established, providing a mathematical basis for optimizing the structural parameters of through-holes. This method effectively captures the system behavior under the synergistic effect of multiple variables by balancing model complexity and computational efficiency.

By fitting the experimental factor combinations and their results in Table 2, a quadratic polynomial regression equation between S21 and the via spacing p, via radius r, and via count n was obtained:

$$S_{21} = -0.0287 - 0.0093 \times A + 0.0171 \times B - 0.0064 \times C + 0.0297 \times AB - 0.0031 \times AC + 0.0113 \times BC - 0.0139 \times A^2 - 0.0186 \times B^2 + 0.01 \times C^2 \tag{15}$$

To ensure the credibility of the regression equation, variance analysis and model significance verification were conducted on the data of equation (15), and the relevant evaluation indicators of the regression equation were obtained. The results are shown in Table 3.

Table 3. Response surface analysis results.

Parameter	Value
F-value	125.18
p-value	⩽0.0001
R2	0.9938
Adjusted R2	0.9859
Predicted R2	0.9012
Adeq Precision	44.3817

According to the data in Table 3, the model p-value obtained from response surface analysis is less than 0.0001 (generally, a value less than 0.05 indicates significance), indicating a significant relationship between the independent variables and the response variable. Both the coefficient of determination (R^2=0.9938) and the adjusted coefficient of determination (Adjusted R^2=0.9859) of the model are close to 1, indicating that the model can explain 98.6% of the variation in the response variable and has a high goodness of fit. The Predicted R^2value is much higher than 0.5, indicating excellent generalization ability of the model and high reliability in predicting new data. The measurement signal-to-noise ratio Adeq Precision is 44.3817, which is much higher

than the threshold value of 4, indicating that the model signal is extremely strong and the noise impact is minimal, making it suitable for optimization and prediction. The above result coefficients all indicate that equation (15) can highly fit the experimental results in Table 3, thus making the regression equation accurate and reliable.

In this experiment, response surface analysis was conducted using Design-Expert software. Based on the experimental results, the variables can be optimized to determine the values of three independent variables that maximize the Coaxial-Like TGV S21 value. The values of the through-hole distance *p*, through-hole radius *r*, and through-hole number n are shown in Fig. 8. In Design-Expert, the optimal values of the independent variables obtained through response surface optimization, along with the analysis of the high-frequency characteristics of Coaxial-Like TGV in the second part, provide important guidance for generating the initial population of the genetic algorithm. These experimentally verified optimization solutions can significantly narrow the search space of the genetic algorithm, improve the fitness of the initial population, and thus accelerate algorithm convergence and avoid falling into local optima. By using the results of statistical optimization as the initial input or reference boundary for the genetic algorithm, the advantages of both methods - the model-driven efficiency of the response surface method and the global search capability of the genetic algorithm - can be combined to further enhance the optimization effect of complex multivariable systems.

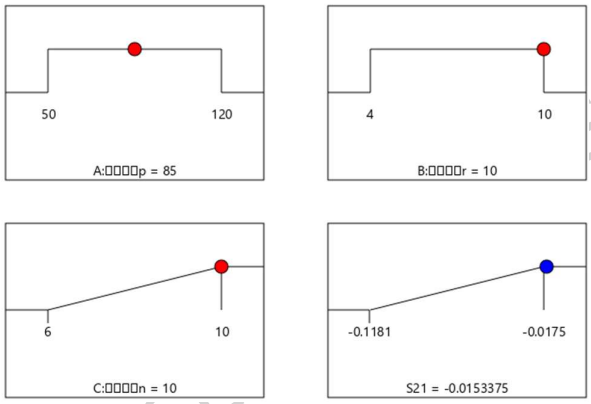

Fig. 8. Values obtained after optimization using response surface methodology.

4.4. Genetic algorithm optimization of Coaxial-Like TGV S21

Genetic algorithms, as a global optimization tool, are commonly applied to the multi-parameter collaborative optimization design of high-frequency electromagnetic structures. By setting the objective function, HFSS combines genetic algorithms to perform an iterative search on geometric parameters, utilizing its global optimization capability to avoid getting stuck in local optima. The algorithm generates a diverse set of solutions by simulating the mechanism of biological evolution, evaluates individual fitness based on the precise full-wave electromagnetic simulation results of HFSS, and Evaluation ultimately converges on the optimal design that satisfies performance constraints. Based on the result parameters affecting Coaxial-Like TGV S21: via spacing p, via radius r, and via count n, a quadratic polynomial regression model between Coaxial-Like TGV structural parameters and its S21 is obtained. The fitting model obtained by optimizing the response surface using genetic algorithms takes the maximum value of Coaxial-Like TGV S21 at 100 GHz as the optimization objective. The objective function value after 50 iterations is shown in Fig. 9. Through optimization using genetic algorithms, the best-performing parameter combination is obtained: p=82.05μm, r=10.44 μm, and *n*=10.

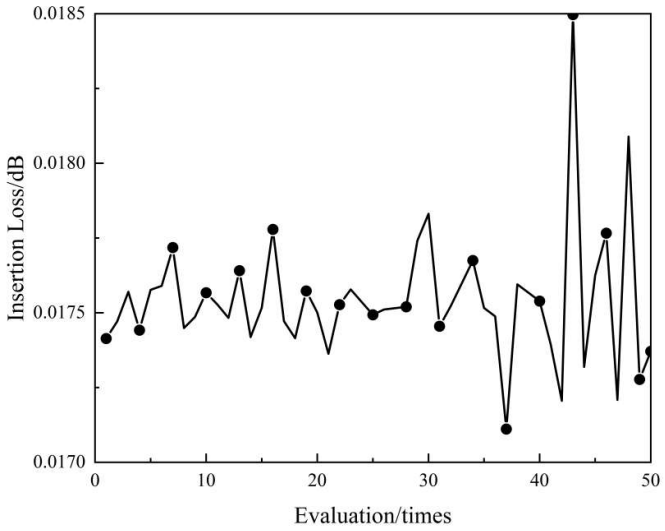

Fig. 9. Objective function value after iteration when n=10.

4.5. Verification of optimized parameter combination for Coaxial-Like TGV S21

The improvement in S21 achieved by the optimized parameter combination (p=82.05 μm, r=10.44μm, and n=10) can be attributed to the following physical mechanisms derived from our equivalent circuit model and electromagnetic analysis:(1) Reduced Inductive Loss and Improved Impedance Matching: The decrease in via pitch p (from the baseline 120 μm) reduces the equivalent loop inductance Lg (Eq. 9), thereby lowering inductive loss. Concurrently, it increases the substrate capacitance C_{sub} (Eq. 12), which improves impedance matching and minimizes signal reflection at high frequencies. (2) Mitigated Conductor Loss: The increase in via radius r enlarges the effective conductive cross-sectional area. This significantly reduces the equivalent resistance Rg (Eq. 6) by alleviating the skin effect at 100 GHz, directly decreasing conductor loss. (3) Enhanced Electromagnetic Shielding: The increase in the number of ground vias n to 10 strengthens the electromagnetic shielding around the signal via. This suppresses field leakage and crosstalk, which is crucial for maintaining signal integrity in the millimeter-wave band.

To verify whether the optimized parameter combination achieves the goal of optimizing Coaxial-Like TGV S21, a three-dimensional electromagnetic simulation model of the Coaxial-Like TGV optimized parameter combination was established, and simulation analysis was conducted under the condition that other conditions remain unchanged. When the parameter combination is p=82.05 μm, r=10.44 μm, and n=10, S21 has a maximum value of -0.0185 dB. The results of Coaxial-Like TGV S21 under the condition of 0~100 GHz are shown in Fig. 11. The red line represents the optimized result, and the black line represents the result before optimization.

According to the results in Fig. 10, within the range of 30~100 GHz, the S21 curve of the optimized parameter combination of Coaxial-Like TGV is higher than that of the basic model (before optimization), indicating a certain degree of optimization of S21. This simulation result aligns with the analysis of the influence of changes in via spacing p, via radius r, and via count n on the trend of S21 variation, and the values of these three variables fall within the range where S21 achieves its maximum value. At 100 GHz, the S21 value of the optimal Coaxial-Like TGV parameter combination is -0.0185 dB, which is 0.0052 dB higher than the S21 value of the basic model (-0.0237 dB), representing an increase of nearly 21.94%, it extends terahertz transmission distance by 2.5%, cuts BER, enhances reliability, reduces array power use by 0.5–1%, and tightens test instrument uncertainty to ±0.01 dB, critical for aerospace/defense. This demonstrates that the S21 obtained with the optimized parameter combination of Coaxial-Like TGV obtained through response surface methodology and genetic algorithm has been significantly improved, achieving optimization of the Coaxial-Like TGV structure.

To elaborate on the practical significance of this 0.0052 dB (21.94%) improvement in insertion loss for RF system performance, we consider its impact in two key aspects. First, in a cascaded multi-stage system (a receiver front-end with filters, low-noise amplifiers, and mixers), every decibel of insertion loss saved at the

interconnect level directly translates into a lower overall system noise figure and improved signal-to-noise ratio (SNR). A reduction of 0.0052 dB, though seemingly small at a single interface, becomes non-negligible when aggregated across dozens or hundreds of such interconnects in a complex 3D-integrated module. Second, in high-power transmission applications (power amplifiers or antenna feeding networks), reduced insertion loss directly decreases dissipated heat, enhancing power efficiency and thermal reliability. For instance, in a 10 W transmit chain, a 0.0052 dB loss reduction saves approximately 0.012 mW of power from being converted into heat per interconnect. While modest per via, this saving scales linearly with both power level and via count, contributing to overall system efficiency and thermal management in densely packed RF systems. Therefore, the achieved optimization, while numerically subtle, represents a meaningful step toward lower-loss, higher-performance interconnects for millimeter-wave 3D integration.

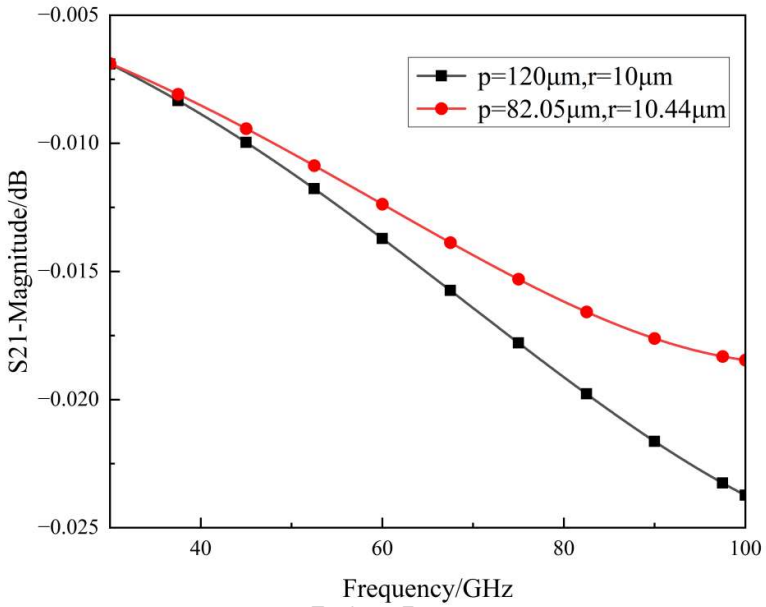

Fig. 10. Comparison of images before and after optimization.

4.6 Comparative Analysis with Other Optimization Algorithms

To further validate the effectiveness and efficiency of the proposed RSM-GA hybrid optimization framework, a comprehensive comparative study was conducted against three other widely-used optimization approaches: a standard Genetic Algorithm (GA), a Multi-Objective Search-based algorithm, and a third algorithm "Search-based". The optimization objective remained consistent with the previous section: minimizing the insertion loss (maximizing S21) at 100 GHz based on the established second-order response surface model (Equation 15). The design variable bounds were fixed as: via pitch p□[80,90] μm, via radius r□[8,11]μm, with the number of ground vias n=10.

All four algorithms were configured with a population size of 30 and terminated after a maximum of 40 generations (evaluations) to ensure a fair comparison of convergence behavior under similar computational budgets. The standard GA used tournament selection, simulated binary crossover (P_c=0.9), and polynomial mutation (P_m=0.1), operating directly on the raw parameter set without a surrogate model. The Multi-Objective Search-based method employed a weighted-sum aggregation technique, while the third "Search-based" algorithm utilized a gradient-free direct search strategy.

Fig. 11 illustrates the convergence trajectories of the four algorithms, plotting insertion loss against the number of function evaluations (calls to the response surface model). As clearly shown, the proposed RSM-GA framework converges most rapidly and stably, reaching a near-optimal insertion loss (approximately 0.02 dB) within only 15–20 evaluations, after which the performance plateaus with minimal fluctuation. In contrast, the standard GA exhibits noticeable oscillations and requires over 30 evaluations to approach a comparable loss level. Both the Multi-Objective Search-based and the Search-based methods demonstrate slower convergence and fail to achieve the same low loss value within the evaluation budget, with the latter showing particularly poor convergence characteristics.

The superior performance of the RSM-GA method stems from the synergistic integration of the Response Surface Model and the Genetic Algorithm. The RSM provides a smooth, analytically tractable surrogate that captures the nonlinear relationship between structural parameters and high-frequency performance, thereby reducing the need for expensive electromagnetic simulations during the optimization loop. This enables the GA to perform a more focused and efficient global search, avoiding the erratic and costly exploration typically observed when optimization algorithms operate directly on a high-dimensional, simulation-based objective landscape. Therefore, the RSM-GA framework proves to be particularly effective for the design optimization of high-frequency interconnect structures such as the Coaxial-Like TGV, where computational efficiency, convergence reliability, and design accuracy are critical.

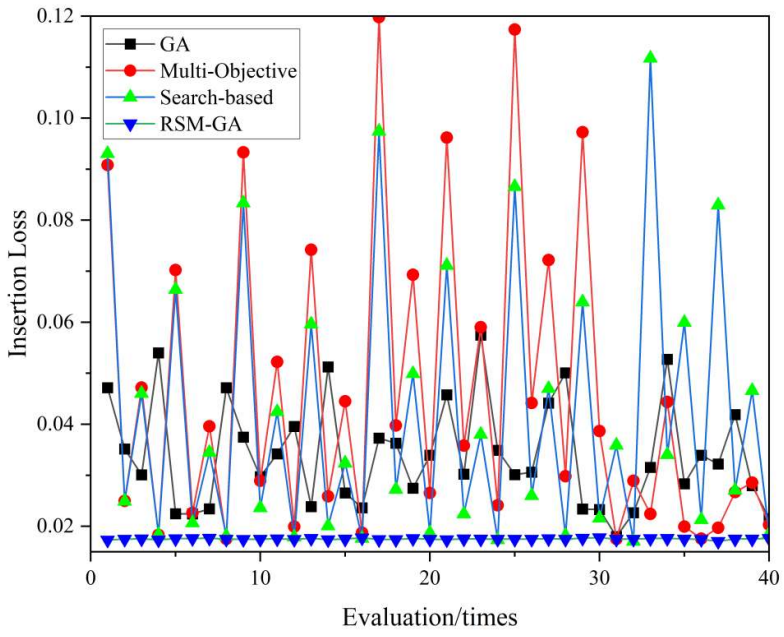

Fig. 11. Convergence comparison of four optimization algorithms: Proposed RSM-GA, Standard GA, Multi-Objective Search-based, and Search-based method, in terms of insertion loss versus number of evaluations.

5. Conclusion

This paper addresses the optimization of high-frequency transmission performance in high-density three-dimensional packaging for Coaxial-Like TGV. By establishing an accurate 3D electromagnetic simulation model, it systematically analyzes the impact mechanism of via spacing, via radius, and the number of ground vias on insertion loss. Furthermore, a collaborative optimization framework combining response surface methodology (RSM) and genetic algorithm (GA) is proposed. Initially, 17 sets of efficient simulation experiments are conducted using Box-Behnken design to construct a high-precision second-order response model, significantly reducing the computational cost of full parameter scanning. Subsequently, GA is employed for global search within the neighborhood of the approximate optimal solution on the response surface, avoiding local optimum traps and ultimately obtaining the optimized parameter combination. Verification through full-wave simulation using HFSS shows that this combination achieves a certain improvement in S21 at the key frequency point of 100 GHz compared to the baseline model. This study provides design criteria for low-loss glass interposers and establishes a hybrid RSM-GA optimization paradigm, which can serve as a reference for the design and optimization of three-dimensional integrated radio frequency devices.Furthermore, a comprehensive comparative analysis with three other optimization algorithms—including a standard GA, a Multi-Objective Search-based method, and a gradient-free search method—confirms that the proposed RSM-GA framework achieves significantly faster convergence and superior optimization accuracy. This validates the efficacy and efficiency of the hybrid approach for the design of high-performance, high-frequency interconnects where computational economy and robust global search are essential.

Acknowledgment

This work was Supported by Guizhou Provincial Basic Research Program (Natural Science) of Youth Guidance (No.〔2025〕241), the Guangxi Science and Technology Base and Talent Special Project: Research and Application of Key Technologies for Precise Navigation (Gui Ke AD25069103), the Foundation Research Project of Kaili University (grant No.YTH-XM2025003), the Open Fund Projct of Qiandongnan Glass Key Laboratory ([2025] WZG02), the Qiandongnan Science and Technology Cooperation Platform([2024] 0001), the Engineering Research Centre of Micro-nano and Intelligent Manufacturing, Ministry of Education (No.[2024] WZG04), and the Science and Technology Breakthrough Project of Hundred Schools and Thousand Enterprises of the Education Department of Guizhou Province (Grant no. QJJ2025011.

Author Contributions

Conceptualization, Shouwei Chen and Xingpeng Liu; Methodology, Shouwei Chen and Jin Wang; Software, Shouwei Chen and Xiaoping Wu; Validation, Shouwei Chen, Jin Wang And Dawen Xia; Formal Analysis, Shouwei Chen; Investigation, Jin Wang; Resources, Shouwei Chen and Jie Liu; Data Curation, Xingpeng Liu and Shouwei Chen; Writing – Original Draft Preparation, Shouwei Chen.; Writing – Review & Editing, Shouwei Chen, Jin Wang, Xingpeng Liu, Jie Liu, Xiaoping Wu and Dawen Xia; Visualization, Shouwei Chen, Jin Wang, Xingpeng Liu and Dawen Xia; Supervision, Dawen Xia; Project Administration, Shouwei Chen and Dawen Xia; Funding Acquisition, Shouwei Chen and Dawen Xia. All authors have read and agreed to the published version of the manuscript.

Data Availability Statement

The data used to support the findings of this study are included within the article.

Conflicts of Interest

The authors declare that they have no competing interest.

References

1 Shen, W.-W. & Chen, K.-N. Three-dimensional integrated circuit (3D IC) key technology: Through-silicon via (TSV). *Nanoscale research letters* **12**, 56 (2017).

2 Kiran, K. M., Kaushik, B. K. & Dhiman, R. Proposal and analysis of coaxial-through-glass vias in 3-D integration using multiresolution time-domain (MRTD) technique. *IEEE Transactions on Components, Packaging and Manufacturing Technology* **14**, 267-276 (2024).

3 Jung, C.-H., Jung, J. P., Sharma, A. & Kim, H.-S. Advanced Through-Glass Via (TGV) Electro-filling and Solder Bumping for Miniaturized 3D MEMS packaging. *Journal of Alloys and Compounds*, 182619 (2025).

4 Engin, A. E. & Narasimhan, S. R. Modeling of crosstalk in through silicon vias. *IEEE transactions on electromagnetic compatibility* **55**, 149-158 (2012).

5 Salah, K. in *2016 3rd International conference on advances in computational tools for engineering applications (ACTEA).* 49-53 (IEEE).

6 Zhao, W.-S. *et al.* Modeling and characterization of coaxial through-silicon via with electrically floating inner silicon. *IEEE Transactions on Components, Packaging and Manufacturing Technology* **7**, 936-943 (2017).

7 Qu, C., Ding, R., Liu, X. & Zhu, Z. Modeling and optimization of multiground TSVs for signals shield in 3-D ICs. *IEEE Transactions on Electromagnetic Compatibility* **59**, 461-467 (2016).

8 Zhang, Y. *et al.* Uniting Integration: Advancing RF Interconnect Technologies. *IEEE Microwave Magazine* **26**, 30-46 (2025).

9 Dong, H. *et al.* Design of a novel compact bandpass filter based on low-cost through-silicon-via technology. *Micromachines* **14**, 1251 (2023).

10 Zhao, Z. *et al.* Electrical characterization of through-silicon-via-based coaxial line for high-frequency 3d integration. *Electronics* **11**, 3417 (2022).

11 Lee, S.-H., Kim, S.-J., Lee, J.-S. & Rhi, S.-H. Thermal Issues Related to Hybrid Bonding of 3D-Stacked High Bandwidth Memory: A Comprehensive Review. *Electronics* **14**, 2682 (2025).

12 Wang, Z., Ye, G., Li, X., Xue, S. & Gong, L. Thermal–mechanical performance analysis and structure optimization of the TSV in 3-D IC. *IEEE Transactions on Components, Packaging and Manufacturing Technology* **11**, 822-831 (2021).

13 Yu, C. *et al.* Application of through glass via (TGV) technology for sensors manufacturing and packaging. *Sensors* **24**, 171 (2023).

14 Yousuf, A. H. B., Hossain, N. M. & Chowdhury, M. H. in *2015 IEEE international symposium on circuits and systems (ISCAS).* 1957-1960 (IEEE).

15 Sukumaran, V., Bandyopadhyay, T., Sundaram, V. & Tummala, R. Low-cost thin glass interposers as a superior alternative to silicon and organic interposers for packaging of 3-D ICs. *IEEE Transactions on Components, Packaging and Manufacturing Technology* **2**, 1426-1433 (2012).

16 Kim, Y. *et al.* Glass interposer electromagnetic bandgap structure for efficient suppression of power/ground noise coupling. *IEEE Transactions on Electromagnetic Compatibility* **59**, 940-951 (2016).

17 Tong, J. *et al.* Electrical modeling and analysis of tapered through-package via in glass interposers. *IEEE Transactions on Components, Packaging and Manufacturing Technology* **6**, 775-783 (2016).

18 Shorey, A., Kuramochi, S. & Yun, C. in *International Symposium on Microelectronics.* 000386-000389 (International Microelectronics Assembly and Packaging Society).

19 Chien, C.-H. *et al.* in *2013 IEEE international 3D systems integration conference (3DIC).* 1-7 (Ieee).

20 Shorey, A. B. & Lu, R. in *2016 Pan Pacific Microelectronics Symposium (Pan Pacific).* 1-6 (IEEE).

21 Lueck, M., Huffman, A. & Shorey, A. in *2015 IEEE 65th Electronic Components and Technology Conference (ECTC).* 672-677 (IEEE).

22 Liu, Y. *et al.* Electromagnetic modeling and analysis of the tapered differential through glass vias. *Microelectronics Journal* **83**, 27-31 (2019).

23 Hu, H. B., Wang, D., Fan, Y. & Cheng, Y. J. in *2023 IEEE MTT-S International Microwave Workshop Series on Advanced Materials and Processes for RF and THz Applications (IMWS-AMP).* 01-03 (IEEE).

24 Liu, J. *et al.* Modeling and Analysis of Parasitic Inductance in TGVs Within High-Density Glass Interposers for High-Speed Interconnects. *IEEE Transactions on Microwave Theory and Techniques* (2025).

25 Lai, Y., Pan, K. & Park, S. Thermo-mechanical reliability of glass substrate and Through Glass Vias (TGV): A comprehensive review. *Microelectronics Reliability* **161**, 115477 (2024).

26 Zhang, G., Chen, H., Yang, Y., Ma, S. & Jin, Y. in *2022 International Conference on Electronics Packaging (ICEP).* 115-116 (IEEE).

27 LeClair, T. & Martin, S. in *54th International Symposium on Microelectronics.* 000149-000153 (International Symposium on Microelectronics).

28 Boora, V., Kumar, A., Kommukuri, M., Chandel, R. & Dhiman, R. Electrical characterization and performance analysis of coaxial through-glass vias. *Sādhanā* **49**, 44 (2024).

29 Kiran, K. M. & Dhimanc, R. Sampling-Biorthogonal Time-Domain Technique for Temperature-Dependent Transient Analysis of Coaxial–TGVs in 3D Integration. *IEEE Transactions on Computer-Aided Design of Integrated Circuits and Systems* (2025).

30 Box G E P, Draper N R. Response surfaces[J]. Mixtures, and Ridge Analyses, 2007, 649.
31 Myers R H, Montgomery D C, Anderson-Cook C M. Response surface methodology: process and product optimization using designed experiments[M]. John Wiley & Sons, 2016.